Volume viscosity and ultrasonic relaxation of ethanol-water mixtures studied by molecular dynamics simulation

Tsuyoshi Yamaguchi
Graduate School of Engineering, Nagoya University, Chikusa, Nagoya, 464–8603, Japan

Corresponding Author:
Tsuyoshi Yamaguchi: yamaguchi.tsuyoshi@material.nagoya-u.ac.jp

Abstract:
The volume viscosity of ethanol-water mixtures at various compositions were calculated by means of equilibrium molecular dynamics simulation, and the results were compared with acoustic experiments. The volume viscosity exhibited a strong maximum around the ethanol mole fraction of 0.27, which is in agreement with experiments. The relaxation in the 100 ps regime, which had been revealed by ultrasonic spectroscopy, was also reproduced. The analysis between the two-body density and the adiabatic pressure fluctuation demonstrated that the large volume viscosity of the mixture originates from the long-range concentration fluctuation.

Graphical Abstract

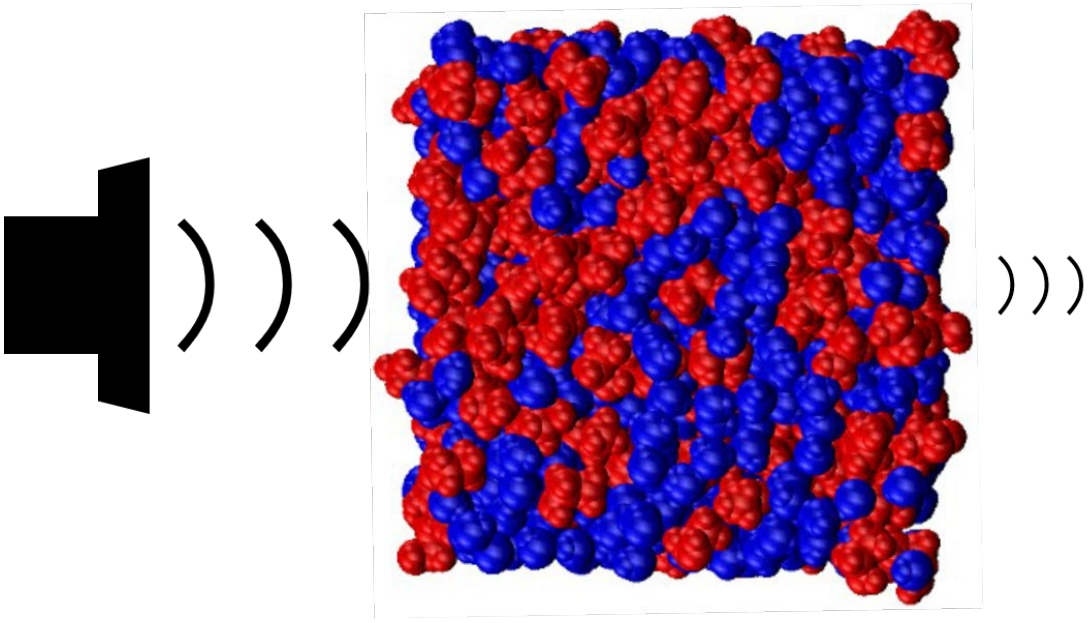

Molecular Dynamics simulation analysis shows that large volume viscosity of ethanol-water mixture is ascribed to long-range concentration fluctuation.

1. INTRODUCTION

Ethanol-water mixture is one of the most famous liquid mixtures for human beings. In addition to its crucial role in improving the quality of our daily life as beverages, its use prevails various fields such as chemical and biological industries, food, medicine, and so on. It has thus been attracting many people including scientific researchers, and there has been a tremendous number of researches on the ethanol-water mixture.

Various macroscopic properties of the ethanol-water mixture have been determined so far. It is well known that the isobaric mixing is thermodynamically exothermic,[1, 2] and accompanies the decrease in volume.[3] The shear viscosity of the mixture is larger than the corresponding values of its constituent neat liquids.[4] Although the experimental results on these properties have been firmly established, their microscopic understandings are still in debate now.

There are two kinds of viscosity in isotropic liquids. One is the shear viscosity defined in terms of the shear stress induced by the shear flow. [5] The term "viscosity" usually refers to the shear viscosity. The other one is the volume viscosity, which is defined as the proportionality coefficient between the compression rate and the isotropic pressure exerted by it. Although the volume viscosity is negligible in hydrodynamic calculations that treats a liquid as an incompressible fluid, it plays an essential role in sound attenuation, and its measurement is possible by means of ultrasonic spectroscopy. [6]

The presence of a maximum in the volume viscosity of ethanol-water mixture is less famous than that of the shear viscosity, but the magnitude of the maximum of the former is far larger than that of the latter. In general, the mixtures of alcohols and water exhibit a large maximum in their volume viscosity, and the magnitude of the maximum increases with increasing the hydrophobicity of the alcohol. [7-9]

The frequency dependence of the volume viscosity can be determined through the measurement of sound velocity and acoustic absorption coefficient as the functions of frequency. The ultrasonic experiments show the dispersion of the volume viscosity of the ethanol-water mixture in the 100 MHz ~ 1 GHz regime, which means that the large volume viscosity of the mixture originates from relaxation processes whose time scales are several hundred ps. [8, 9]

There have been many mechanisms proposed so far for the large volume viscosity of ethanol-water mixture. For example, chemical reaction model was applied assuming stoichiometric complex formation between ethanol and water molecules.[10, 11] A model based on the coupling between pressure and long-range concentration fluctuation was proposed and tested. [12-14] The theory of sound absorption of critical mixture was extended to this non-critical mixture. [9] The scattering of ultrasound by short-lived clusters was also considered as the reason for the sound attenuation.[8] However, the experimental results have been reproduced to some degree by quite different models, and there is no definite proof for the mechanism of the volume viscosity. Due to the lack of the established mechanism, it is still unclear what the characteristic strong ultrasonic absorption tells us on the microscopic structure and dynamics of ethanol-water mixture.

The ultrasonic spectroscopy possesses a unique character that it probes microscopic processes through

the coupling with volume and enthalpy.[6] Since most chemical processes accompany the changes in volume or enthalpy, the ultrasonic spectroscopy has an advantage in a sense because it can probe processes that is not detected by other experimental methods such as optical and magnetic resonance spectroscopies. However, such a characteristic becomes a disadvantage of the ultrasonic spectroscopy as a lack of selectivity. Since so many microscopic processes can be candidates to account for an observed relaxation, the assignment is sometimes impossible by experiment alone. The combination with theoretical and computational studies are thus desirable, for which methodologies to analyze the frequency-dependent volume viscosity are indispensable. This work constitutes our efforts to develop such methodologies, taking a famous experimental result on ethanol-water mixture as an example.

In this work, molecular dynamics (MD) simulation of ethanol-water mixture at various compositions was performed to clarify the microscopic origin of volume viscosity. Equilibrium MD simulation runs were performed, and the volume viscosity was calculated from the time correlation function of the adiabatic pressure fluctuation using Kubo-Green theory. After confirming that the maximum of the volume viscosity was reproduced, the analysis of the mechanism was performed through the cross correlation between the adiabatic pressure fluctuation and the two-body density, as we performed for the analysis of shear viscosity of various liquids including neat liquid methanol.[15-17]

2. THEORY

Kubo-Green theory describes linear transport coefficients in terms of the time-correlation functions of the corresponding currents in equilibrium systems, which can be evaluated by equilibrium MD simulation. For example, shear viscosity, η_s, of isotropic liquid is given by the time correlation function of the shear stress, P_{xy}, as[18]

$$\eta_s = \int_0^\infty dt\, G(t) \ , \tag{1}$$

$$G(t) \equiv \frac{V}{k_B T} \langle P_{xy}(0) P_{xy}(t) \rangle \ , \tag{2}$$

where k_B, T, and V denote the Boltzmann constant, the absolute temperature, and the volume of the system, respectively.

The Kubo-Green expression of the volume viscosity, η_v, is[19-21]

$$\eta_v = \int_0^\infty dt\, K(t) \ , \tag{3}$$

$$K(t) \equiv \frac{V}{k_B T} \langle \delta P'(0) \delta P'(t) \rangle \ , \tag{4}$$

where $\delta P'$ stands for the adiabatic fluctuation of isotropic pressure. An important point is that, contrary to the shear stress in eq. (2), the expression of $\delta P'$ depends on the ensemble of the system. In the constant-energy constant-volume (NVE) ensemble, $\delta P'$ equals to the ordinary pressure fluctuation. In the constant-temperature constant-volume (NVT) ensemble, which is employed in this work, the expression of $\delta P'$ is given by

$$\delta P'(t) = \delta P(t) - \frac{\langle \delta P \delta E \rangle}{\langle |\delta E|^2 \rangle} \delta E(t), \tag{5}$$

where δP and δE mean the fluctuations of the pressure and the total energy. Eq. (5) states that contribution of the energy fluctuation to the pressure fluctuation through the coupling with heat bath should be projected out for the calculation of volume viscosity, which is reasonable considering the adiabatic nature of sound wave in the hydrodynamic limit. The coefficient of $\delta E(t)$ in eq. (5) is usually described in terms of the derivative of pressure with respect to energy, and the equivalence of the two expressions are shown in Sec. S1 of Supporting Information.

In our recent works, we proposed a method to analyze the microscopic mechanism of shear viscosity by calculating the cross-correlation function of the two-body density with the shear stress. [15] The real space representation of the two-body density is given by

$$\rho_{\alpha\gamma}^{(2)}(\boldsymbol{r}) \equiv \sum_{j\in\alpha, j'\in\gamma} \delta\big(\boldsymbol{r}_j - \boldsymbol{r}_{j'} - \boldsymbol{r}\big), \tag{6}$$

where α and γ refer to the species of the sites in the liquid, such as the oxygen atom of water. Its equilibrium average is related to the partial radial distribution function, $g_{\alpha\gamma}(\boldsymbol{r})$, as

$$\langle \rho_{\alpha\gamma}^{(2)}(\boldsymbol{r}) \rangle \equiv \rho_\alpha \delta_{\alpha\gamma} \delta(\boldsymbol{r}) + \rho_\alpha \rho_\gamma g_{\alpha\gamma}(|\boldsymbol{r}|), \tag{7}$$

where ρ_α means the number density of the site α. The partial radial distribution function is a popular representation of equilibrium liquid structure. The fluctuation of $\rho_{\alpha\gamma}^{(2)}(\boldsymbol{r})$,

$$\delta\rho_{\alpha\gamma}^{(2)}(\boldsymbol{r}) \equiv \rho_{\alpha\gamma}^{(2)}(\boldsymbol{r}) - \langle \rho_{\alpha\gamma}^{(2)}(\boldsymbol{r}) \rangle, \tag{8}$$

is then regarded as the transient fluctuation of the liquid structure.

It is sometimes useful to employ the reciprocal-space representation of the two-body density,

$$\tilde{\rho}_{\alpha\gamma}^{(2)}(\boldsymbol{q}) \equiv \tilde{\rho}_\alpha^*(\boldsymbol{q}) \tilde{\rho}_\gamma(\boldsymbol{q}), \tag{9}$$

$$\tilde{\rho}_\alpha(\boldsymbol{q}) \equiv \sum_{j\in\alpha} \exp\big(i\boldsymbol{q}\cdot\boldsymbol{r}_j\big), \tag{10}$$

rather than the real-space representation, eq. (6). Its equilibrium average gives the static structure factor as

$$\tilde{\chi}_{\alpha\gamma}(|\boldsymbol{q}|) = \frac{1}{V}\langle \tilde{\rho}_{\alpha\gamma}^{(2)}(\boldsymbol{q}) \rangle, \tag{11}$$

and the fluctuation of $\tilde{\rho}_{\alpha\gamma}^{(2)}(\boldsymbol{q})$ is defined similarly to eq. (8) as the deviation from the average.

As we have proposed for the shear viscosity, the cross correlation between the adiabatic pressure fluctuation and the transient two-body density at different times gives information on the structural relaxation modes that govern the volume viscosity. The expressions of the cross-correlation functions analyzed in this work are described as follows:

$$\rho_{v,\alpha\gamma}^{(2)}(|\boldsymbol{r}|, t) \equiv \langle \delta P'(0) \delta\rho_{\alpha\gamma}^{(2)}(\boldsymbol{r}, t) \rangle, \tag{12}$$

$$\tilde{\rho}_{v,\alpha\gamma}^{(2)}(|\boldsymbol{q}|, t) \equiv \langle \delta P'(0) \delta\tilde{\rho}_{\alpha\gamma}^{(2)}(\boldsymbol{q}, t) \rangle. \tag{13}$$

3. COMPUTATIONAL METHODS

MD simulation runs of ethanol-water mixtures were performed at various values of the molar fraction of ethanol, x_E = 0, 0.1, 0.2, 0.27, 0.4, 0.6, 0.8, and 1. All the simulation runs were performed under the NVT ensemble. The temperature was fixed to be 298.15 K using Nosé-Hoover thermostat,[22] and the volume of

the system was taken from experiment at the same temperature and composition.[3] The average pressures calculated by MD simulation were shown in Fig. S1 of Supporting Information. We employed OPLS-AA and TIP4P/2005 models for ethanol and water, respectively.[23, 24] The total number of the molecules in the systems was 1000. An MD run of 8000 molecule system was also performed at $x_E = 0.27$ to examine the system size dependence. A production run of 1 μs length was performed for each system after the equilibration run of 100 ns length. The molecules were confined within a cubic cell with the periodic boundary condition, whose dimension was determined by the experimental molar volume.

The equation of motion was integrated using leapfrog algorithm with the time step of 1 fs. The bond lengths and the bond angle of water were fixed by the SETTLE algorithm.[25] For ethanol, the lengths of bonds associated with an H atom were fixed by the LINCS algorithm,[26] and other bond lengths and bond angles were treated as flexible. The long-range part of the Coulombic interaction was treated by the particle-mesh Ewald method,[27] and the short-range interactions, including the Lennard-Jones one, were cut off at 1.2 nm. All the MD simulation runs were performed by using GROMACS software package.[28]

Provided that the dynamics of total energy is involved in the NVT expression of the adiabatic pressure fluctuation, eq. (5), one may consider that the obtained value of the volume viscosity may be affected by the thermostat. In Nosé-Hoover method, the coupling strength between the system and the heat bath is characterized by the time constant of the thermostat, τ_{bath}. The shorter value of τ_{bath} means the stronger coupling. We tested the five values of τ_{bath}, 0.5, 5, 50, 500 and 5000 ps, at $x_E = 0.27$, and found that the variation of η_v with τ_{bath} is within the acceptable range considering the statistical error, as will be shown in the next section. Therefore, we fixed the value of $\tau_{bath} = 0.5$ ps to ensure the sufficient temperature control.

4. RESULTS AND DISCUSSION

The values of the shear and volume viscosity obtained by our MD simulation are plotted as the function of x_E in Fig. 1. Both η_s and η_v exhibit a maximum at the intermediate value of x_E. Their experimental values are also shown in Fig. 1 for comparison. The experimental value of η_s is taken from a literature.[4] The experimental volume viscosity of mixtures is calculated from the fitting function of the frequency-dependence of the ultrasonic absorption coefficient reported by Brai and Kaatze,[9] and the value of neat water was taken from the review of Kaatze and coworkers. [6]

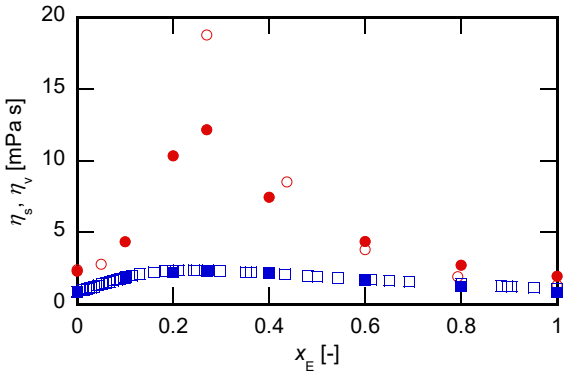

FIGURE 1. The volume viscosity (η_v, red circles) and the shear viscosity (η_s, blue squares) are plotted as the functions of the molar fraction of ethanol, x_E. The values obtained in our present MD simulation are shown with filled symbols, whereas the experimental values taken from the literatures [4, 6, 9] are with open ones.

The agreement between MD simulation and experiment is very good for shear viscosity. There have been many MD simulation works on the shear viscosity of the mixture of ethanol and water using various molecular models. Guevara-Carrion and co-workers demonstrated that the concentration dependence of the shear viscosity is reproduced well by using the TIP4P/2005 model for water.[29] By contrast, the results of MD simulation using TIP4P and OPLS-AA models were not so good. [30] We thus consider that our present result also supports the good performance of TIP4P/2005 model for the shear viscosity of aqueous mixtures. The agreement in volume viscosity is worse, particularly in that the maximum value is underestimated in our MD simulation. However, our MD simulation nicely captures the characteristics of the concentration dependence of the volume viscosity, because the concentration of the maximum volume viscosity is reproduced and the increase of the volume viscosity on mixing is much larger than that of the shear viscosity.

The running integral of the correlation functions, $G(t)$ and $K(t)$ defined by eqs. (2) and (4), respectively, are plotted in Fig. 2. The value of x_E is 0.27, where the volume viscosity exhibits a maximum in Fig. 1. Their respective limiting values at $t \to \infty$ give η_s and η_v. The experimental $K(t)$ is reconstructed from the ultrasonic absorption spectrum of Brai and Kaatze,[9] and plotted together in Fig. 2 for comparison. The corresponding experimental results on $G(t)$ is not available, because experimental techniques to measure the complex shear viscosity in the GHz frequency range is still under development now.[31]

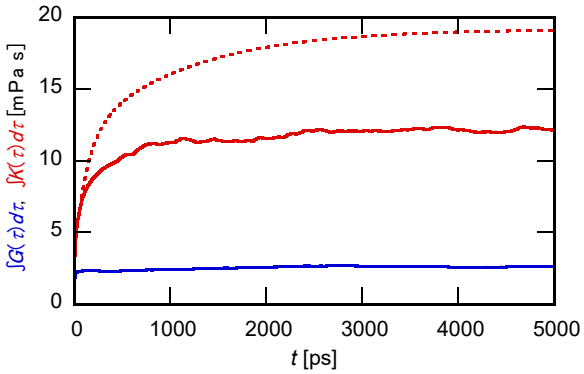

FIGURE 2. The running integrals of $G(t)$ (blue) and $K(t)$ (red). The simulation results are drawn with the solid curves, whereas the experimental $K(t)$ is with the dotted one.

According to Fig. 2, $G(t)$ and $K(t)$ from the simulation exhibit the dynamics quite different from each other. The former is almost converged within 100 ps, while the latter shows a slow relaxation in the time scale of 100 ps. The slow relaxation of $K(t)$ is also visible in the ultrasonic experimental result. Although the relaxation rate is faster and the relaxation amplitude is smaller in our MD simulation, we consider that our MD simulation captures the characteristics of the slow relaxation of the adiabatic pressure fluctuation.

The different dynamics of $G(t)$ and $K(t)$ suggests that the microscopic dynamic modes that determine the volume viscosity and the shear viscosity are different. In particular, the mechanism of the maximum of volume viscosity might be different from that of shear viscosity.

Before going to the detailed analysis of the relaxation process that gives the volume viscosity, we examine the possible influence of the thermostat to the relaxation dynamics and the integrated value of volume viscosity. The examination was performed at $x_E = 0.27$, where the volume viscosity exhibits the maximum. MD simulation runs with the five different values of the time constant of the thermostat, 0.5, 5, 50, 500, and 5000 ps, were performed, and $K(t)$ was calculated from each run.

The running integrals of $K(t)$ were plotted and compared with each other in Fig. 3. The relaxation dynamics within 1 ns scarcely depends on the time constant of the thermostat. Although some differences are found at later time, there is no tendency between the integrated value of $K(t)$ and the time constant, and we consider that the difference is within the statistical error of our MD simulation. Therefore, we performed the runs at different concentrations with the time constant of 0.5 ps, in order to confirm the sufficient thermostatting.

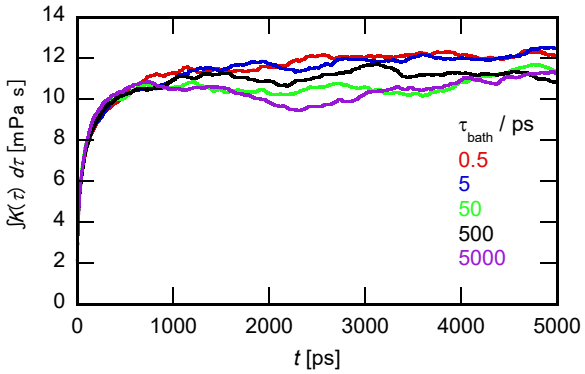

FIGURE 3. The running integrals of $K(t)$ at $x_E = 0.27$ and different coupling strength of the thermostat. The values of the time constant of the thermostat are, $\tau_{bath} = 0.5$ (red), 5 (blue), 50 (green), 500 (black), and 5000 ps (purple), respectively.

The adiabatic pressure fluctuation defined by eq. (5) consists of the fluctuations of pressure and total energy. Although the results are not shown for brevity, the time profiles of the autocorrelation functions of both terms strongly depend on the time constant. Both autocorrelation functions exhibit an oscillatory behavior, and the period of the oscillation increases with increasing the time constant. However, the oscillation is cancelled by taking the linear combination in eq. (5), and invisible in the resultant $K(t)$. Therefore, it can be said that the projection in eq. (5) succeeds in excluding the effects of the artificial thermostat. As will be shown later, in addition, the memory of the adiabatic pressure fluctuation is stored in the configurational space, whereas it is the momentum space that is directly coupled to the thermostat. We consider it is another reason why the thermostat makes a marginal influence to the relaxation dynamics of $K(t)$.

The running integrals of $K(t)$ at various concentrations are compared in Fig. 4. Their long-time limiting values correspond to η_v exhibited in Fig. 1. The most important point in Fig. 4 is that the slow relaxation mode in the 100 ps time scale is absent in neat liquids, $x_E = 0$ and 1, and the volume viscosity of the mixture larger than those of its constituent neat liquids is ascribed to the presence of the slow mode. The slow relaxation mode of $K(t)$ is thus ascribed to the dynamics specific to liquid mixture. Comparing the time profiles of the mixtures at different compositions, the variation of the relaxation rate of the slow mode is rather small, and the variation of the amplitude is mainly responsible to the concentration dependence of the volume viscosity. The weak concentration dependence of the relaxation time is consistent with the experimental relaxation times determined by Brai and Kaatze.[9]

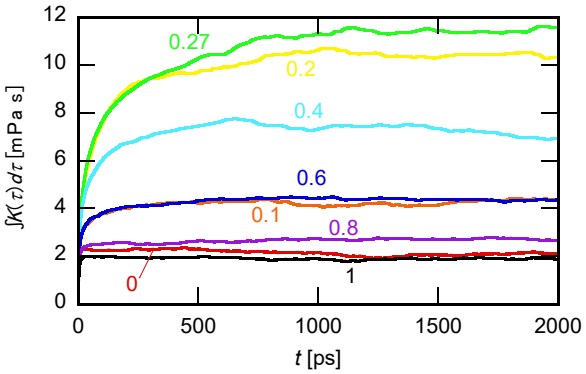

FIGURE 4. The running integrals of $K(t)$ at various concentrations. The values of the molar fraction of ethanol are, $x_E = 0$ (red), 0.1 (orange), 0.2 (yellow), 0.27 (green), 0.4 (aqua), 0.6 (blue), 0.8 (purple), and 1 (black), respectively, which are shown in the panel with the corresponding colors.

Hereafter, we shall try to extract the microscopic origin of the slow relaxation in $K(t)$ by means of the cross correlation between the adiabatic pressure fluctuation and the two-body density introduced in Sec. 2.

Fig. 5 shows the partial radial distribution functions between the oxygen atoms at $x_E = 0.27$. The oxygen sites of water and ethanol are hereafter denoted as O_W and O_E, respectively. The three components, O_W-O_W, O_W-O_E, and O_E-O_E, are plotted together. The strong peaks are observed at $r = 0.28$ nm in all the pairs due to the direct hydrogen bonds. The strongest peak of the water-water pair means that water molecules are likely to cluster together in the mixture. In addition, the distributions between the same species (O_W-O_W and O_E-O_E) are larger than the O_W-O_E one at distances from 0.5 to 0.8 nm. Therefore, the attractive tendency between the same species is inferred from the partial radial distribution functions.

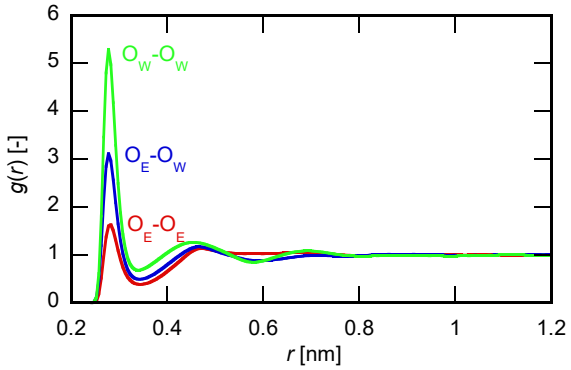

FIGURE 5. The partial radial distribution functions between oxygen atoms at $x_E = 0.27$. The functions between ethanol-ethanol (red), ethanol-water (blue), and water-water (green) are exhibited.

The time-integrated profiles of $\rho^{(2)}_{v,\alpha\gamma}(|\boldsymbol{r}|, t)$ at the same composition, $x_E = 0.27$, are shown in Fig. 6. The time integral is performed from $t = 0$ to 2 ns, where $K(t)$ is almost converged. The distributions between

the oxygen atoms are plotted as the partial radial distribution function, Fig. 5. In Fig. 6, all the three components exhibit long-range distributions. The correlations with the pair densities between the same species, O_E-O_E and O_W-O_W, are positive, whereas that with the O_E-O_W pair is negative. It clearly demonstrates that the adiabatic pressure fluctuation is coupled to the long-range concentration fluctuation. The idea of the coupling between the concentration fluctuation and pressure variation is consistent with the concentration fluctuation model proposed by Romanov and Solov'ev.[12, 13] The positive sign of the pairs of the same species indicates that the demixing of the two species is promoted by the adiabatic compression. Thermodynamic experiments show that the isothermal-isobaric mixing of water and ethanol accompanies the decrease in molar volume.[3] The transient demixing due to the thermal fluctuation thus leads to the increase in pressure under the isochoric condition, which is consistent with the cross-correlation functions shown in Fig. 6.

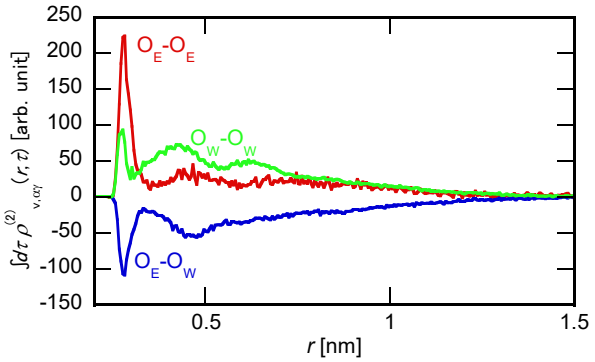

FIGURE 6. The coupling between the two-body density and the adiabatic pressure fluctuation, $\rho^{(2)}_{v,\alpha\gamma}(|\boldsymbol{r}|,t)$ integrated over time from $t = 0$ to 2 ns. The O_E-O_E, O_E-O_W, and O_W-O_W components are drawn with the red, blue, and green curves, respectively.

Considering that the profiles of $\rho^{(2)}_{v,\alpha\gamma}(|\boldsymbol{r}|,t)$ in Fig. 6 are diffuse and long-ranged, we consider that the analysis is better performed in the reciprocal space, rather than the cluster analysis in the real space. In addition, the reciprocal space representation is convenient to consider the relation with the concentration fluctuation model and the critical mixture model. Therefore, we define the concentration mode in the reciprocal space as

$$\tilde{\rho}_c(\boldsymbol{q}) \equiv x_E \tilde{\rho}_{O_W}(\boldsymbol{q}) - (1 - x_E)\tilde{\rho}_{O_E}(\boldsymbol{q}). \tag{14}$$

The two-body density and its cross correlation with the adiabatic pressure fluctuation are also defined as

$$\tilde{\rho}^{(2)}_{cc}(\boldsymbol{q}) \equiv \tilde{\rho}^{*}_{c}(\boldsymbol{q})\tilde{\rho}_c(\boldsymbol{q}), \tag{15}$$

$$\tilde{\chi}_{cc}(|\boldsymbol{q}|) \equiv \frac{1}{V}\langle \tilde{\rho}^{(2)}_{cc}(\boldsymbol{q})\rangle, \tag{16}$$

$$\tilde{\rho}^{(2)}_{v,cc}(|\boldsymbol{q}|,t) \equiv \langle \delta P'(0)\delta\tilde{\rho}^{(2)}_{cc}(\boldsymbol{q},t)\rangle. \tag{17}$$

The concentration mode $\tilde{\rho}_c(\boldsymbol{q})$ defined by eq. (14) is proportional to those used in the analysis of small-angle X-ray or neutron scattering[32, 33] as is described in Sec. S3 of Supporting Information.

The cross-correlation functions $\tilde{\rho}^{(2)}_{v,cc}(|\boldsymbol{q}|,t)$ of the mixture of x_E = 0.27 at various values of t are exhibited in Fig. 7. A strong coupling is observed in the low-q region, q < 5 nm^{-1}, from the initial time, t = 0. Although the coupling is also found at higher q, the decay of the coupling with the short-range structures is almost completed within 100 ps, and only the low-q concentration fluctuation survives at longer time. Since the long-range concentration fluctuation decays through the mutual diffusion, its decay rate increases with increasing q. As a result, the width of the low-q peak of $\tilde{\rho}^{(2)}_{v,cc}(|\boldsymbol{q}|,t)$ decreases with time, as is demonstrated in Fig. 7.

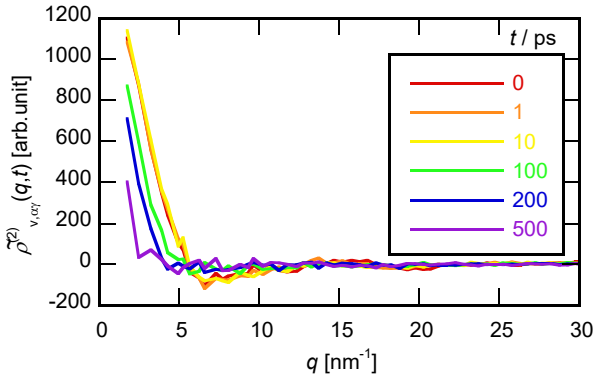

FIGURE 7. $\tilde{\rho}^{(2)}_{v,cc}(|\boldsymbol{q}|,t)$ of the mixture of x_E = 0.27 at various times. The values of t are, 0 (red), 1 (orange), 10 (yellow), 100 (green), 200 (blue), and 500 ps (purple), respectively. The first three curves are almost overlapped with one another at q < 5 nm^{-1}.

Two equilibrium functions, $\tilde{\chi}_{cc}(q)$ and $\tilde{\rho}^{(2)}_{v,cc}(|\boldsymbol{q}|,t=0)$, of all the mixtures studied in this work are plotted in Fig. 8 to clarify the origin of the concentration dependence of the volume viscosity. The functions for neat liquids, x_E = 0 and 1, are not shown because they are zero by definition.

According to Fig. 8a, the structure factor of the concentration fluctuation, $\tilde{\chi}_{cc}(|\boldsymbol{q}|)$, shows a peak around q = 0, indicating the long-range concentration fluctuation. The presence of the q = 0 peak has been reported experimentally by means of small-angle X-ray or neutron scattering, and ascribed to the concentration fluctuation.[33] The q = 0 limit of $\tilde{\chi}_{cc}(|\boldsymbol{q}|)$ gives the thermodynamic concentration fluctuation of an open system as

$$N\langle|\delta x_E|^2\rangle = x_E(1-x_E)\frac{\tilde{\chi}_{cc}(q=0)}{\tilde{\chi}_{cc}(q\to\infty)}, \tag{18}$$

where N stands for the total number of molecules in the system, and the left-hand side of eq. (18) is related to the osmotic compressibility. The small-angle X-ray scattering experiment performed by Nishikawa and Iijima showed that the water-ethanol mixture at 293 K exhibits a peak of the concentration fluctuation at x_E = 0.4, and its maximum value is about 1.0.[32] In Fig. 8a, the concentration of the maximum fluctuation is around x_E = 0.4, as was reported by Nishikawa and Iijima. However, the maximum value of $N\langle|\delta x_E|^2\rangle$ at x_E = 0.4 is about 0.5, contrary to the experimental value of 1.0. Therefore, our MD simulation appears to

underestimate the magnitude of the concentration heterogeneity of water-ethanol mixtures.

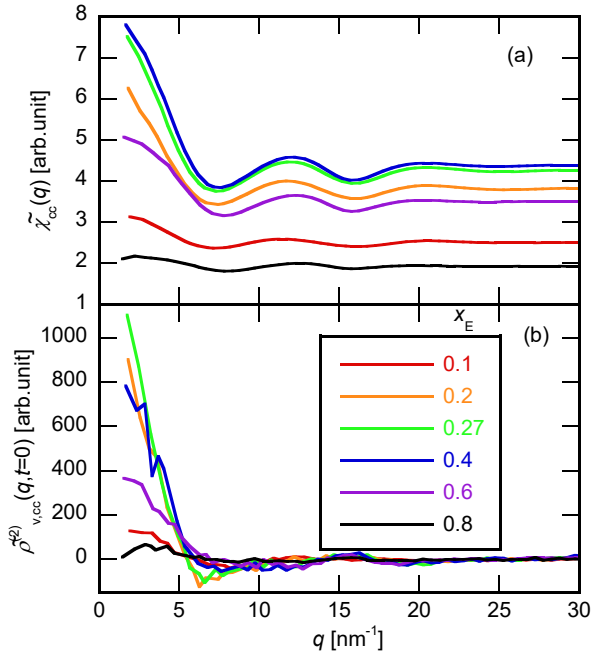

FIGURE 8. (a) $\tilde{\chi}_{cc}(q)$ and (b) $\tilde{\rho}^{(2)}_{v,cc}(q, t = 0)$ of the mixtures at various compositions. The values of x_E are 0.1 (red), 0.2 (orange), 0.27 (green), 0.4 (blue), 0.6 (purple), and 0.8 (black), respectively.

The coupling between the adiabatic pressure fluctuation and the concentration fluctuation at t = 0 is exhibited in Fig. 8b. The coupling at low-q region, q < 5 nm^{-1}, is dominant at all the compositions, and the peak height changes with the composition. An important point is that the composition of the maximum coupling in Fig. 8b is x_E = 0.27, which is different from that of the maximum concentration fluctuation, x_E = 0.4. The concentration of the maximum volume viscosity corresponds to that of the maximum coupling strength between the pressure and the concentration fluctuation, rather than that of the maximum concentration fluctuation. The difference in the concentrations of the maximum volume viscosity and the maximum concentration fluctuation has been known well in experiments. Romanov and Solov'ev applied their concentration fluctuation model to the volume viscosity of ethanol-water mixture, estimating the coupling strength between the pressure and the concentration fluctuation from the curvature of the excess mixing molar volume, and succeeded in reproducing the concentration of maximum volume viscosity. [12, 13] Based on the discussion above, we consider that the results of our present MD simulation support the concentration fluctuation model by Romanov and Solov'ev.

Another point to be noted is that the widths of the q = 0 peak of $\tilde{\chi}_{cc}(q)$ and $\tilde{\rho}^{(2)}_{v,cc}(|\boldsymbol{q}|, t = 0)$ in Fig. 8 are rather broad to be regarded as the critical concentration fluctuation, and the narrowing of the peak is not so evident around the concentration of the maximum volume viscosity. Therefore, we consider that the models based on the critical concentration fluctuation may not be appropriate for the volume viscosity of

ethanol-water mixture. Brai and Kartze applied the critical concentration model for the ultrasonic relaxation spectra of ethanol-water mixtures, and found that the correlation length obtained from their parameter optimization was extremely small, below 1 nm.[9] We consider that the short correlation length is then in harmony with the broad peaks at $q = 0$ in Fig. 8. In addition, the weak dependence of the width of the $q = 0$ peak on composition is consistent with the small variation of the relaxation rate shown in Fig. 4.

Given the importance of the long-range concentration fluctuation revealed in this work, one may suspect that the system size of our present MD simulation, 1000 molecules, is insufficient. As is shown in Fig. 1, our present MD simulation underestimates the maximum value of the volume viscosity. In Fig. 2, the relaxation time of $K(t)$ is also underestimated. Since concentration fluctuation whose length scale is larger than the simulation cell is not included, the contribution of long-range and slow concentration fluctuation is missing in our MD simulation, which might explain the quantitative disagreement between our simulation and experiment. In order to test the influence of the system size, we also performed an MD simulation run of 8000 total molecules at $x_E = 0.27$. The running integrals of $G(t)$ and $K(t)$ obtained by 1000 and 8000 molecule systems are compared in Fig. 9. The results of these two systems are close to each other. In particular, the difference in the running integral of $K(t)$ is far smaller than that between the simulation and the experiment. Although the results are not shown for brevity, the cross-correlation functions between the adiabatic pressure fluctuation and the two-body density in both systems are close to each other. Therefore, we consider that the present system size of 1000 total molecules is sufficiently large, and the finite system size of the MD simulation is not a principal reason for the discrepancy between the simulation and the experiment.

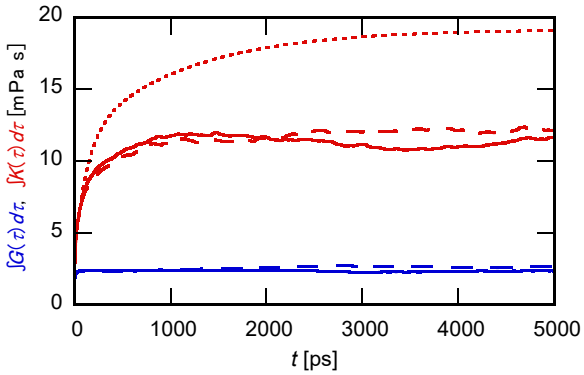

FIGURE 9. The running integrals of $G(t)$ (blue) and $K(t)$ (red). The simulation results of 1000 and 8000 molecule systems are drawn with the dashed and the solid curves, respectively, whereas the experimental $K(t)$ is with the dotted one.

In Figs. 7 and 8, the correlation functions in the reciprocal space do not converge to constant values even at the smallest value of q in our simulation of 1000 molecules, 1.9 ($x_E = 0.1$) – 1.4 ($x_E = 0.8$) nm^{-1}. One may thus consider that the contribution of the lower q is missing in our simulation, and that strong

system size dependence is expected, contrary to the rather weak size dependence shown in Fig. 9. We consider that it is because the contribution of $\tilde{\rho}_{v,cc}^{(2)}(|\boldsymbol{q}|,t)$ to $K(t)$ should be weighted by the volume factor in the reciprocal space, $4\pi q^2$. The contribution of the fluctuation at lower q to the volume viscosity is suppressed by the q^2 factor compared with the expectation from large cross correlation in $\tilde{\rho}_{v,cc}^{(2)}(|\boldsymbol{q}|,t)$.

Then, what is the reason for the quantitative disagreement between the simulation and the experiment? We showed in Fig. 8a that the magnitude of the concentration fluctuation in our simulation is about half of the experimental one at x_E = 0.4, and we consider it is a reason for the underestimation of the volume viscosity of the mixtures. Since the volume viscosity is shown to be caused by the concentration fluctuation, the underestimation of the magnitude of the latter naturally leads to that of the former. The increase in the concentration fluctuation also retards the relaxation of the fluctuation through the thermodynamic factor of the mutual diffusion coefficient.[34] The underestimation of the concentration fluctuation means that the hydrophobicity of the OPLS-AA ethanol in TIP4P/2005 water is smaller than that of the real system, although we cannot specify at present what part of the force field should be improved. The underestimation of the coupling strength between the pressure and the concentration fluctuations can also be a reason for the underestimation of the volume viscosity. According to Fig. S1, however, the mean pressure behaves as a convex function of x_E, which means that the magnitude of the isobaric mixing volume is larger in this model than in experiment. Since the coupling strength is thermodynamically given by the second derivative of the mixing volume, the coupling should be rather stronger in the present model. The combination of the TIP4P/2005 and the OPLS-AA models describes the concentration dependence of the shear viscosity well. However, since the microscopic mechanism of the volume viscosity is different from that of the shear viscosity as is suggested by Fig. 2, the excellent success in the shear viscosity might not mean the suitability for the volume viscosity.

Although our present MD simulation was performed at a fixed temperature, 298.15 K, it would be interesting to investigate the temperature dependence of the volume viscosity in the future work. D'Arrigo and Paparelli measured the ultrasonic absorption coefficients of ethanol-water mixtures in the whole concentration range at the temperatures from -40 to 30 °C, and found that the maximum of the absorption coefficient becomes more pronounced at the lower temperature.[14] They analyzed their experimental results based on the theory of Romanov and Solov'ev, and the stronger sound absorption at the lower temperature is ascribed to the smaller mutual diffusion coefficient that governs the relaxation of the concentration fluctuation. The slower relaxation of the concentration relaxation at the lower temperature will require longer MD simulation runs, and the independent evaluation of the mutual diffusion coefficient including the thermodynamic factor would also be required for the detailed verification of the mechanism.

5. SUMMARY

We performed MD simulation on ethanol-water mixtures and calculated the volume viscosity as a function of composition. We succeeded in reproducing the large increase in the volume viscosity on mixing,

and the presence of the slow relaxation mode in the ultrasonic absorption spectrum in the 100 ps time scale was also reproduced. The origin of the volume viscosity was analyzed based on the cross-correlation function between the adiabatic pressure fluctuation and two-body density functions. The analysis demonstrated the strong coupling between the adiabatic pressure fluctuation and the long-range concentration fluctuation, which clearly supports the concentration fluctuation model proposed by Romanov and Solov'ev. The transient compression by ultrasound causes microscopic demixing of the two components, and the relaxation of the demixing results in the attenuation of the ultrasound.

Conflicts of interest

There is no conflict of interests to declare.

ACKNOWLEDGMENTS

We are grateful for financial support from JSPS KAKENHI (Grant Nos 19H02677 and 19K03768).

Data Availability Statement

The data that support the findings of this study are available from the corresponding author upon reasonable request.

References

1. R. F. Lama and B. C. Y. Lu, *J. Chem. Eng. Data*, 1965, **10**, 216-219.
2. J. A. Boyne and A. G. Williamson, *J. Chem. Eng. Data*, 1967, **12**, 318-318.
3. H. A. Zarei, F. Jalili and S. Assadi, *J. Chem. Eng. Data*, 2007, **52**, 2517-2526.
4. R. L. Kay and T. L. Broadwater, *J. Solution Chem.*, 1976, **5**, 57-76.
5. R. B. Bird, W. E. Stewart and E. N. Lightfoot, *Transport Phenomena*, Wiley, New York, 2nd edn., 2007.
6. U. Kaatze, T. O. Hushcha and F. Eggers, *J. Solution Chem.*, 2000, **29**, 299-368.
7. M. J. Blandamer and D. Waddington, *Adv. Mol. Relax. Processes*, 1970, **2**, 1-40.
8. U. Kaatze, M. Brai and K. Menzel, *Ber. Bunsenges. Phys. Chem.*, 1994, **98**, 1-8.
9. M. Brai and U. Kaatze, *J. Phys. Chem.*, 2002, **96**, 8946-8955.
10. L. R. O. Storey, *Proc. Phys. Soc. B*, 1952, **65**, 943-950.
11. K. Takagi and K. Negishi, *Jpn. J. Appl. Phys.*, 1975, **14**, 953-960.
12. V. P. Romanov and V. A. Solov'ev, *Sov. Phys. Acoust.*, 1965, **11**, 68-71.
13. V. P. Romanov and V. A. Solov'ev, *Sov. Phys. Acoust.*, 1965, **11**, 219-220.
14. G. D'Arrigo and A. Paparelli, *J. Chem. Phys.*, 1988, **88**, 7687-7697.
15. T. Yamaguchi and A. Faraone, *J. Chem. Phys.*, 2017, **146**, 244506.
16. T. Yamaguchi, *J. Phys. Chem. B*, 2018, **122**, 1255-1260.
17. T. Yamaguchi, *Phys. Chem. Chem. Phys.*, 2018, **20**, 17809-17817.
18. J.-P. Hansen and I. R. McDonald, *Theory of Simple Liquids*, Academic Press, London, 2nd edn., 1986.
19. J. A. McLennan, *Prog. Theor. Phys.*, 1963, **30**, 408-409.
20. R. Zwanzig, *Annu. Rev. Phys. Chem.*, 1965, **16**, 67-102.
21. P. L. Palla, C. Pierleoni and G. Ciccotti, *Phys. Rev. E*, 2008, **78**, 021204.
22. M. P. Allen and D. J. Tildesley, *Computer Simulation of Liquids*, Clarendon Press, Oxford, 1987.
23. W. L. Jorgensen, D. S. Maxwell and J. Tirado-Rives, *J. Am. Chem. Soc.*, 1996, **118**, 11225-11236.
24. J. L. Abascal and C. Vega, *J. Chem. Phys.*, 2005, **123**, 234505.
25. S. Miyamoto and P. A. Kollman, *J. Comput. Chem.*, 1992, **13**, 952-962.
26. B. Hess, H. Bekker, H. J. C. Berendsen and J. G. E. M. Fraaije, *J. Comput. Chem.*, 1997, **18**, 1463-1472.
27. U. Essmann, L. Perera, M. L. Berkowitz, T. Darden, H. Lee and L. G. Pedersen, *J. Chem. Phys.*, 1995, **103**, 8577-8593.
28. M. J. Abraham, T. Murtola, R. Schulz, S. Páll, J. C. Smith, B. Hess and E. Lindahl, *SoftwareX*, 2015, **1-2**, 19-25.
29. G. Guevara-Carrion, J. Vrabec and H. Hasse, *J. Chem. Phys.*, 2011, **134**, 074508.
30. E. J. W. Wensink, A. C. Hoffmann, P. J. van Maaren and D. van der Spoel, *J. Chem. Phys.*, 2003,

119, 7308-7317.

31. T. Yamaguchi and T. Matsuoka, *Jpn. J. Appl. Phys.*, 2021, DOI: 10.35848/1347-4065/ac4141.
32. K. Nishikawa and T. Iijima, *J. Phys. Chem.*, 2002, **97**, 10824-10828.
33. K. Nishikawa, *Bull. Chem. Soc. Jpn.*, 2021, **94**, 2170-2186.
34. Y. Zhou and G. H. Miller, *Phys. Rev. E*, 1996, **53**, 1587-1601.